Ultrasound in Med. & Biol., Vol. 48, No. 1, pp. 124–142, 2022

0301-5629/$ - see front matter

https://doi.org/10.1016/j.ultrasmedbio.2021.09.004

● *Original Contribution*

ACOUSTIC CHARACTERIZATION OF TISSUE-MIMICKING MATERIALS FOR ULTRASOUND PERFUSION IMAGING RESEARCH

Peiran Chen,[A] Andreas M.A.O. Pollet,[B] Anastasiia Panfilova,[A] Meiyi Zhou,[A] Simona Turco,[A] Jaap M.J. den Toonder,[B] and Massimo Mischi[A]

[a] Dept. Electrical Engineering, Eindhoven University of Technology, Eindhoven, Netherlands; and [b] Dept. Mechanical Engineering, Institute for Complex Molecular Systems, Eindhoven University of Technology, Eindhoven, Netherlands

(*Received* 13 *April* 2021; *revised* 3 *September* 2021; *in final form* 3 *September* 2021)

Abstract—Materials with well-characterized acoustic properties are of great interest for the development of tissue-mimicking phantoms with designed (micro)vasculature networks. These represent a useful means for controlled *in-vitro* experiments to validate perfusion imaging methods such as Doppler and contrast-enhanced ultrasound (CEUS) imaging. In this work, acoustic properties of seven tissue-mimicking phantom materials at different concentrations of their compounds and five phantom case materials are characterized and compared at room temperature. The goal of this research is to determine the most suitable phantom and case material for ultrasound perfusion imaging experiments. The measurements show a wide range in speed of sound varying from 1057 to 1616 m/s, acoustic impedance varying from 1.09 to 1.71 × 10^6 kg/m^2s, and attenuation coefficients varying from 0.1 to 22.18 dB/cm at frequencies varying from 1 MHz to 6 MHz for different phantom materials. The nonlinearity parameter B/A varies from 6.1 to 12.3 for most phantom materials. This work also reports the speed of sound, acoustic impedance and attenuation coefficient for case materials. According to our results, polyacrylamide (PAA) and polymethylpentene (TPX) are the optimal materials for phantoms and their cases, respectively. To demonstrate the performance of the optimal materials, we performed power Doppler ultrasound imaging of a perfusable phantom, and CEUS imaging of that phantom and a perfusion system. The obtained results can assist researchers in the selection of the most suited materials for *in-vitro* studies with ultrasound imaging. (E-mail: p.chen1@tue.nl) **© 2021 The Author(s). Published by Elsevier Inc. on behalf of World Federation for Ultrasound in Medicine & Biology. This is an open access article under the CC BY license (http://creativecommons.org/licenses/by/4.0/).**

Keywords: **acoustic properties, tissue-mimicking materials, case materials, perfusable phantoms, ultrasound perfusion imaging.**

INTRODUCTION

Imaging and quantification of blood perfusion reveals a fundamental property of tissue that varies in many important physiological and pathological processes (Cosgrove and Lassau, 2010). Current methods for perfusion imaging by ultrasound are based on Doppler ultrasound and contrast-enhanced ultrasound (CEUS). Doppler ultrasound is a noninvasive imaging modality that can be used to estimate the blood perfusion in blood vessels. Conventional Doppler ultrasound techniques, such as continuous-wave Doppler, are based on the Doppler effect, enabling the quantification of blood flow by observing the spectrum of Doppler frequencies at the receiver (Dymling et al., 1991). Color flow imaging (CFI) provides real-time view of blood flow in terms of mean flow velocity and direction using color mapping (Szabo, 2014). As a variation of CFI, power Doppler (ultrasound angiography) is based on the power of the signal coherence that is estimated by autocorrelation over frames, improving the ability over standard CFI to image blood flow in smaller vessels (Szabo, 2014). More recently, leveraging the development of high-frame-rate imaging and plane-wave imaging, vector Doppler technique provides the velocity vector in all directions of blood flow by dedicated apodization (Szabo, 2014). Due to the complexity of flow and vascular architecture, there is a need to assess the accuracy of flow measurements and the sensitivity of flow imaging in small vessels when designing novel Doppler ultrasound techniques. Therefore, *in-vitro* test and validation in vascular phantoms

Corresponding to: Peiran Chen, Flux 7.078, Eindhoven University of Technology, De Groene Loper 19, 5612AP, Eindhoven, Netherlands. E-mail: p.chen1@tue.nl

for which the flow distribution is accurately known are necessary. CEUS provides real-time imaging of blood flow with the help of intravenously-injected ultrasound contrast agents (UCAs). These consist of gas-filled microbubbles encapsulated in a biocompatible shell with the size comparable to that of blood cells (Cosgrove, 2006). Thanks to their size, they behave as blood-pool agents and thus are suitable to assess blood flow dynamics down to the micro-circulation. Several advanced techniques have been proposed for quantification of perfusion in a broad range of clinical applications, especially in cardiology, radiology, and oncology. Quantification methods are often based on empirical or physics-driven modeling of the UCA flow kinetics, leading to the estimation of parameters related to blood flow and velocity (Mischi et al., 2018; Turco et al., 2020). However, although *in-vivo* studies have shown promising results (Mischi et al., 2012; Feinstein, 2004; van Sloun et al., 2017; Kuenen et al., 2011; Wildeboer et al., 2018), the relationship between the underlying (micro)vascular architecture and the UCA kinetics, along with the resulting CEUS image enhancement and ultimately the estimated hemodynamic parameters is not well understood.

In this context, perfusable phantoms are an essential tool for developing ultrasound perfusion imaging techniques and performing *in-vitro* validation. In the past years, tissue-mimicking phantoms, which have been used to mimic biological tissues, have played a pivotal role in experimental studies supporting the development of clinical ultrasound solutions, such as performance testing of ultrasound imaging systems (Culjat et al., 2010; Zell et al., 2007), skills training in medical ultrasonography (Culjat et al., 2010; Richardson et al., 2015; Dabbagh et al., 2014), and experimental investigation of blood-flow dynamics with ultrasound imaging systems (Kenwright et al., 2015; Meagher et al., 2007). Materials with well-characterized acoustic properties are of great interest for the development of these phantoms.

The quality of ultrasound imaging is highly sensitive to the propagation of ultrasound waves in scanned materials; therefore, in principle, such phantom materials should exhibit acoustic properties similar to those of water and typical soft tissues in the human body, as shown in Table 1 (Culjat et al., 2010; Cao et al., 2017). Typically, acoustic properties such as speed of sound (SoS), acoustic impedance (Z) and attenuation coefficient (α) are considered (Culjat et al., 2010; Cao et al., 2017; Madsen et al., 1982; Cafarelli et al., 2017; Zell et al., 2007). For instance, materials with acoustic impedance that largely differs from the acoustic impedance of water will produce strong reflections and shadowing, leading to a degraded image of the phantom interior. Materials with high attenuation also result in a poor imaging quality due to the low power of the received echoes. This aspect is particularly relevant for CEUS, where low acoustic pressures are employed to minimize bubble destruction. The recommended values of SoS and α are 1540 m/s and 0.3-0.7 dB/cm/MHz, respectively (AIUM Technical Standards Committee 1990; American Institute of Ultrasound in Medicine 1992) (Browne et al., 2003; Madsen et al., 1998).

In addition to the aforementioned properties, the acoustic nonlinearity of materials is also relevant, especially in the context of CEUS imaging. CEUS imaging enhances the ultrasound signals from microbubbles (UCAs) dispersed in blood by exploiting the nonlinear behavior of UCAs compared to tissues; therefore, tissue-mimicking materials with high nonlinearity lead to decreased contrast-to-tissue ratio. The parameter of nonlinearity (B/A) quantifies the nonlinear propagation effects of acoustic waves in materials, describing how a propagating finite-amplitude acoustic wave progressively distorts when travelling through a medium (Gong et al., 1989; Law et al., 1985). Its value varies from 5.0 to 12.0 for several biological tissues such as liver, fatty tissue and heart as shown in Table 1.

In this study, the investigated materials aim at being used to fabricate (micro)vasculature phantoms for ultrasound perfusion imaging and for investigation of flow dynamics in the (micro)vasculature; thus, a clearly-visible (micro)vascular structure in the phantom is of great

Table 1. Acoustic properties of typical soft tissues.

Material	Speed of sound SoS (m/s)	Mass density ρ (kg/m^3)	Acoustic impedance Z (10^6 kg/m^{2}s)	Attenuation α (dB/cm/MHz)	Nonlinearity B/A	Source
Fat	1478	950	1.4	0.48	10.8	(Gong et al., 1989; Mast, 2000)
Breast	1510	1020	1.54	0.75	-	(ICRU, 1998)
Kidney	1560	1051	1.64	1.0	7.4	(Mast, 2000)
Cardiac muscle	1576	1060	1.67	0.52	7.1	(Mast, 2000; ICRU, 1998)
Liver	1595	1060	1.69	0.5	6.6	(Mast, 2000; ICRU, 1998)
Water	1480	1000	1.48	0.0025	5.2	(Dong et al., 1999; Havlice and Taenzer, 1979)

interest, which serves as the reference of the ultrasound perfusion imaging. To ensure the visibility, we do not seed the phantom materials to mimic realistic acoustic scatters; therefore, the backscatter strength is not included in the investigated acoustic property list. In addition to the investigated acoustic properties, the optical transparency of perfusable phantom materials is another desirable feature, which ensures that flow in the perfusable phantoms can be visualized by optical imaging systems such as micro Particle-Image Velocimetry. The flow patterns obtained by optical imaging systems can then be employed as a reference for comparing perfusion imaging results in relevant *in-vitro* ultrasound investigations.

In an effort to determine the optimal phantom materials, we investigated materials currently used for *in-vitro* tissue-mimicking phantoms, *in-vivo* tissue substitutes, ultrasound therapy, microfluidic devices, and in the biotechnology industry. With the constraint that materials for perfusable phantoms should be easy to fabricate, and compatible with both ultrasound perfusion imaging and optical imaging, the following set of fabricated materials was selected for further investigation: gelatin, agarose, polyacrylamide (PAA), polydimethylsiloxane (PDMS), polyvinyl alcohol (PVA), alginate and polyethylene glycol diacrylate (PEGDA).

Gelatin is a homogeneous colloid gel that has been widely used as tissue-mimicking material. Examples are phantoms mimicking human organs including cysts (Madsen et al., 1980; Bude and Adler, 1995) or gelatin-based materials mixed with oil to mimic body fat (Madsen et al., 1982). Gelatin is often selected due to its low cost, good acoustic properties and easy preparation (Madsen et al., 1978; Bude and Adler, 1995). However, gelatin's main disadvantages are its weak structural properties, short life-time, and instability at various temperatures (Ophir et al., 1981), even while being stored in a refrigerator under a humid environment.

Agarose is a hydrophilic colloid derived from agar. Agar-based and agarose-based materials have been widely used for mimicking soft tissue (Zell et al., 2007; Maxwell et al., 2010), as well as for manufacturing breast ultrasound phantoms (Cannon et al., 2011). Agarose is a cheap material that is easy to use; however, its short life-time and low optical transparency limit its use.

PAA, an acrylic hydrogel that is made by chemical cross-linking, is mostly used for gel electrophoresis and manufacturing of contact lenses. In the ultrasound domain, PAA was investigated as an acoustic coupling medium for focused ultrasound therapy (Prokop et al., 2003). PAA has good acoustic properties similar to those of the human breast tissue and skin (Zell et al., 2007). Moreover, PAA is a strong, easy-to-use and transparent material. PAA have stringent requirements on storage, similar to gelatin and agarose. As mentioned in (Zell et al., 2007), PAA is possibly toxic.

PDMS is a silicone rubber, which is often used for the fabrication of microfluidic devices and microelectromechanical systems (Genchi et al., 2013). PDMS shows several advantages including stability at normal temperature and normal humidity, long-term re-usage and visual transparency. Additionally, PDMS is a high-cost material.

PVA is typically employed as biodegradable container material. It has recently been exploited as a tissue-mimicking material due to its high structural rigidity, longevity, bio-compatibility and non-toxicity (Zell et al., 2007; Fromageau et al., 2003; Kharine et al., 2003). By nature it is non-transparent, which hampers the optical imaging of PVA phantoms. The protocol for fabricating transparent and strong phantoms of PVA is more complicated (Cha et al., 1992).

Alginate is widely used in bioengineering and in the biotechnology industry owing to its biocompatibility (Salsac et al., 2009; Lee et al., 2013). It is a natural polysaccharide derived from brown seaweed and can form thermally stable and biocompatible hydrogel material by cross-linking using calcium or another bivalent cation. Alginate is mostly used as an encapsulation medium in a form of hydrogel bead, but its use for the production of large phantoms is difficult. The material is not transparent.

PEGDA is a synthetic material with hydrophilicity and relative inertness. It is often referred as a "blank slate" in biomedical applications since it does not interact with the body until modified. To produce PEGDA, cross-linking is achieved by using a photoinitiator and light (Caliari and Burdick, 2016). The material is low-cost, transparent, but it has low mechanical stability.

The aforementioned materials are candidates for fabricating (micro)vascular phantoms. Since all of them are soft hydrogels, their mechanical stiffness is low. To overcome this issue, the realized phantoms are often enclosed in a rigid case. A full enclosure casing avoids deformation of the soft hydrogel inside the case while being imaged; this is of particular interest for research in ultrasound perfusion imaging as it prevents changes of position and geometry of the (micro)vasculature while imaging, and ensures reliable perfusion in the soft hydrogels phantoms. Therefore, in this paper, the acoustic properties of a set of case materials to support the hydrogels for easy handling and long-term storage are also investigated. Phantoms enclosed in a case can be connected to input and output ports of the case to allow perfusion of the phantom. Possible case materials are polycarbonate (PC), polymethyl methacrylate (PMMA), polymethylpentene (TPX), cyclic olefin copolymer (COC) and polyether block amide (PEBA). All of them are optically transparent and have a high mechanical

strength. The phantoms and their cases compose the perfusion system, which can be finally used for *in-vitro* experiments with ultrasound perfusion imaging.

In this paper, we present results of a series of experiments based on the introduced seven types of phantom materials and five types of case materials, and systematically compare their acoustic properties including SoS, Z, α and B/A. For each phantom material, we prepared a set of different concentrations by dissolving corresponding material compounds in MilliQ water. The transmitted ultrasound frequency ranged from 1 MHz to 6 MHz with 1-MHz interval. For the experimental setup, the pulse transmission approach was adopted (Madsen et al., 1982; Cafarelli et al., 2017; Dong et al., 1999; Shui et al., 2008; Gong et al., 1989), transmitting long pulses with a narrow bandwidth, avoiding overlap between the harmonics in the received spectrum. The optimal material should have acoustic properties close to that of human soft tissues; especially for the case material, low attenuation is preferred. The transparency is necessary for the optimal material. Good longevity and stability, and a relatively easy preparation protocol would be desired choice. Thus, in order to quantitatively determine the optimal material, a scoring system is designed to rank all the materials in terms of their speed of sound, acoustic impedance, attenuation, nonlinearity, transparency, life-time, stiffness, as well as preparation protocol, as shown in Table 2. Additionally, after identifying the optimal phantom and case materials, we compared CEUS imaging in phantoms made of optimal and unsuitable materials, as well as power Doppler ultrasound imaging in phantoms made of optimal and unsuitable materials. Moreover, an example of perfusion system and the corresponding CEUS image are also presented. This paper gives a systematic comparison of phantom materials including not only typically used materials such as gelatin and agarose, but also acrylamide which is less common. The measurements of the nonlinearity of the phantom materials provide more comprehensive information, not fully investigated in existing work. The comparison of nonlinearity of different phantom materials can provide useful information for relevant research such as phantom-based ultrasound nonlinearity imaging. Moreover, the investigation of the case materials evidences that the rigid phantom case is also suitable for ultrasound imaging in addition to soft hydrogels, solving the challenges in connecting tubing for perfusion without leakage typically encountered with soft hydrogels. By ranking the materials using the designed scoring system, we determine that the optimal phantom material is PAA at a concentration of 20% and optimal case material is TPX.

Table 2. Scoring system for ranking materials.

Parameter	Scoring criteria
Speed of sound (phantom and case)	1510 - 1595 m/s: 10 points (soft hydrogel) 1400 - 2000 m/s: 10 points (stiff case material) Deviation: 1 point less per 10 m/s
Acoustic impedance (phantom and case)	1.54 - 1.69 $\times$ 10^6 kg/m^{2}s: 10 points (soft hydrogel) 1.40 - 2.00 $\times$ 10^6 kg/m^{2}s: 10 points (stiff case material) Deviation: 1 point less per 1 $\times$ 10^4 kg/m^{2}s
Attenuation (phantom and case)	0.5 - 0.75 dB/cm/MHz: 10 points Deviation: 1 point less per 0.8 dB/cm averaged over the frequency range
B/A (phantom only)	5.0 - 12.0 : 10 points Deviation: 1 point less per 1
Transparency (phantom and case)	Transparent: 10 points Half-transparent: 5 points Non-transparent: 0 point
Life time (phantom and case)	Stable and long: 10 points Long but has storage requirements: 5 points Short: 0 point
Stiffness (phantom and case)	Stiff: 10 points Soft: 5 points
Preparation protocol (phantom only)	Typical material: 10 points Less common material: 5 points Require extra processing: 3 points less

MATERIALS AND METHODS

Material preparation

The investigated phantom materials include gelatin with concentration of 7.5%, 10% and 15%, agarose with concentration of 2%, 3% and 5%, PAA with concentration of 5%, 7.5%, 10%, 15% and 20%, PDMS with concentration ratio of 10:1, PVA with concentration of 10%, 15% and 20%, alginate with concentration of 1% and 3%, and PEGDA with concentration of 15% and 20%. All the phantom material samples were casted in glass Petri dishes with a diameter of 55 mm, resulting in disc-like samples with thickness of about 15 mm for most of the phantom materials. The thickness of each sample was measured by vernier caliper while performing acoustic measurement.

Gelatin from bovine skin type b (G9391, Sigma-Aldrich, Zwijndrecht, Netherlands) was dissolved in MilliQ water at 7.5%, 10% and 15% wt at 60 degrees Celsius. After complete dissolution, samples were casted and cooled to room temperature before solidification at 4 degrees Celsius. The measured thickness of 7.5%, 10% and 15% gelatin were about 11.7 mm, 16.0 mm, and 16.0 mm, respectively.

Ultrapure agarose (16500500, Thermofisher, Waltham, Massachusetts, USA) was dissolved in MilliQ water at 2%, 3% and 5% wt at 100 degrees Celsius. After complete dissolution, samples were casted at 90 degrees Celsius and cooled to room temperature to solidify. The measured thickness of 2%, 3% and 5% agarose were about 16.8 mm, 16.8 mm, and 11.8 mm, respectively.

PAA was made by combining acrylamide (A, A8887, Sigma-Aldrich, Zwijndrecht, Netherlands) (5%, 7.5%, 10%,

15% and 20% wt) with N,N'-Methylenebisacrylamide solution (2%) (B-A, M1533, Sigma-Aldrich, Zwijndrecht, Netherlands) (10%, 15%, 20%, 30% and 40% volume) and adding Ammonium persulfate (AP, A3678, Sigma-Aldrich, Zwijndrecht, Netherlands) (0.05% wt for all samples) and N,N,N',N'-Tetramethylethylenediamine (TEMED, T9281, Sigma-Aldrich, Zwijndrecht, Netherlands) (0.15% volume) in MilliQ water. Directly after adding AP and TEMED, the samples were casted and covered by a glass plate to prevent air inhibiting the cross-linking reaction and ensuring a flat surface (Cafarelli et al., 2017). The measured thickness of 5%, 7.5%, 10%, 15% and 20% PAA were about 11.0 mm, 14.3 mm, 13.6 mm, 14.3 mm and 15.7 mm, respectively.

PDMS (Sylgard 184, Dow Corning, Midland, Michigan, USA) was made by combining base and curing agent in a 10:1 ratio and stirring vigorously. The material was degassed, casted and degassed again to remove all air bubbles from the material. The curing was done at 65 degrees Celsius for 2 hours. The measured thickness of 10:1 PDMS was about 9.4 mm.

PVA (mw 130.000, 563900, Sigma-Aldrich, Zwijndrecht, Netherlands) was made by dissolving 20% wt PVA in a mixture of 80% wt dimethyl sulfoxide (DMSO, Sigma-Aldrich, Zwijndrecht, Netherlands)/ 20% wt MilliQ water at 120 degrees Celsius for 1 hour while stirring. The PVA solution was casted after all air bubbles had disappeared from the liquid and it was cooled to room temperature. Solidification was done by keeping the samples overnight at -20 degrees Celsius, resulting in a transparent hydrogel. The solvent was washed out by submerging the sample in MilliQ water and replacing it everyday for 3 days (Cha et al., 1992; Funamoto et al., 2014). The measured thickness of 10%, 15% and 20% PVA were about 12.4 mm, 10.6 mm and 10.5 mm, respectively.

Sodium alginate (180947, Sigma-Aldrich, Zwijndrecht, Netherlands) was dissolved in mother saline at concentrations of 1% and 3% w/v overnight under continuous stirring. Mother saline consists of MilliQ water with 154 mnM Sodium Chloride (NaCl, 746398, Sigma-Aldrich, Zwijndrecht, Netherlands) and 10 mM HEPES buffer solution (HEPES, 83264, Sigma-Aldrich, Zwijndrecht, Netherlands). The alginate solution was frozen into shape (-18 degrees Celsius) before submerging it in gelation solution for 48 hours in a fridge at 4 degrees Celsius. Gelation solution consists of mother saline with addition of 115 mM Calcium Chloride (CaCl, 746495, Sigma-Aldrich, Zwijndrecht, Netherlands) (Salsac et al., 2009). The measured thickness of 1% and 3% alginate were about 4.7 mm and 8.8 mm, respectively.

PEGDA (Mn 700, 455008, Sigma-Aldrich, Zwijndrecht, Netherlands) was dissolved at 10%, 15% and 20% (v/v) in buffer solution consisting of MilliQ water with 10 mM HEPES, 100 mM NaCl and 1.5% (v/v) triethanolamine (TEOA, 90279, Sigma-Aldrich, Zwijndrecht, Netherlands). As photo-initiators 0.35% (v/v) 1-Vinyl-2-pyrrolidinone (VP, V3409, Sigma-Aldrich, Zwijndrecht, Netherlands) and 1% (v/v) 1 mM Eosin Y disodium salt (Eosin, E6003, Sigma-Aldrich, Zwijndrecht, Netherlands) were added. Cross-linking was achieved using white light (KL 2500 LCD, Schott, Colombes, France) for 15 minutes (Heintz et al., 2016, Heintz et al.,2017). The measured thickness of 15% and 20% PEGDA were about 15.0 mm and 14.9 mm, respectively.

All the phantom material samples were stored at 4 degrees Celsius in a Petri dish with additional water to prevent dehydration.

The case material samples were thinner than the casted phantom material samples. The case material PMMA (Epraform, Eriks, Alkmaar, Netherlands) and PC (Arla Plast AB, Eriks, Alkmaar, Netherlands) samples were cut from plate material with thickness of 2 mm. TPX (MX001, GF56787036, Sigma-Aldrich, Zwijndrecht, Netherlands) pellets were compression molded into 2-mm plate material for testing at a temperature of 280 degrees for 30 minutes. COC (TOPAS 6013, TOPAS Advanced Polymers GmbH, Frankfurt am Main, Germany) 5-mm thick and PEBA (PEBAX Clear 1200 and PEBAX 3533 SA01, Arkema, Colombes, France) 2-mm thick samples were obtained from the suppliers and used without further modification.

Acoustic measurement

The through-transmission technique was used to measure the acoustic properties of the tissue-mimicking phantom materials and case materials (Cafarelli et al., 2017). In this technique, water is employed as a reference by comparing ultrasonic waves propagating through water with ultrasonic waves propagating through the prepared material samples, submerged in water. The comparison provides a measurement of the materials' acoustic properties based on the known acoustic properties of water. As depicted in Figure 1, the experimental set-up consists of a plane piston source and receiver.

In order to measure the acoustic properties (SoS, Z and α) in a frequency range varying from 1 MHz to 6 MHz, we divided the measurements into two sets. In the first set of measurements, we employed two transducers (V306 with a diameter of 13 mm and C304 with a diameter of 25 mm; Panametrics, Olympus Inc., Waltham, MA, USA) with 2.25-MHz center frequency to transmit and receive. Ultrasonic waves ranging from 1 MHz to 3 MHz with 10 cycles and 0.25 ms time interval were transmitted. In the second set, we employed two transducers (V309 with a diameter of 13 mm and V307 with a diameter of 25 mm; Panametrics, Olympus Inc., Waltham, MA, USA) with 5-MHz center frequency. Ultrasonic waves ranging

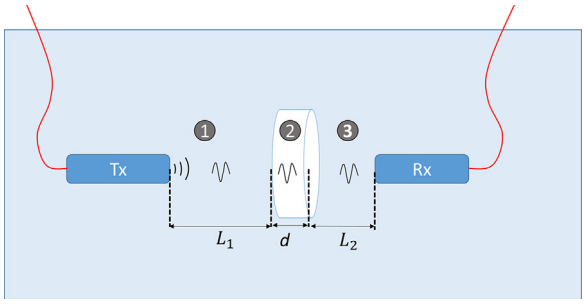

Figure 1. Experimental scheme: transmitted (Tx) ultrasound signals go to the receiver (Rx), passing through three parts: (1) water with interval distance L_1, (2) sample with thickness d, (3) water with interval distance L_2.

from 4 MHz to 6 MHz with 10 cycles and 0.25 ms time interval were transmitted. Moreover, an extra transmission at 3.5 MHz was conducted in both sets to validate the measurement consistency. In both sets, the transducers were driven by a 33220A arbitrary wave generator (Agilent Technologies, Santa Clara, California, USA), connected to a 50-dB 2100L RF Power amplifier (Acquitek, Massy, France). A dedicated Labview program (National Instruments Corp., Austin, TX, USA) was employed to control the wave generator. The received signals were displayed on a TDS2014 oscilloscope (Tektronix, UK limited, Bracknell, UK) and further sampled by an NI-5122 (National Instruments Corp.) acquisition board at 25 MHz. Both the transmitter and receiver were fixed on a dedicated rail system, and the samples were fixed in a dedicated frame which was located on the rail system, between the transducers. The transducers and samples were aligned along their longitudinal axis, ensuring that the beam can exactly penetrate through the samples. Moreover, the transmitted acoustic pressure amplitudes were lower than 40 kPa, as measured by using an 1.0-mm needle hydrophone (Precision Acoustics Ltd, UK), avoiding the formation of harmonics when measuring the attenuation. The material sample with thickness d measured by vernier scale was placed in between.

The SoS of materials was calculated using:

$$\mathrm{SoS} = \frac{d}{\Delta t + \frac{d}{\mathrm{SoS}_w}}, \tag{1}$$

where SoS_w (1497 m/s) is the speed of sound in water at room temperature, and Δt is the difference in the ultrasound propagation time from transmitter to receiver between the two conditions with and without sample. The time difference Δt was estimated by maximizing the cross-correlation between the received signals in the presence and absence of the sample.

Based on the calculated SoS, the acoustic impedance (Z) was calculated by:

$$Z = \mathrm{SoS} \cdot \rho, \tag{2}$$

where ρ is the material density. The density of all the investigated materials, with relative sources, are provided in Appendix A.

The attenuation coefficient (α) is a frequency-dependent parameter. Here, α was measured at seven (1:1:6 MHz, and 3.5 MHz) different frequencies according to (Mischi et al., 2014):

$$\alpha = 0.0025 f^2 - 8.686 \frac{1}{d} \ln \frac{A_s}{A_w T}. \tag{3}$$

where f is the frequency of the transmitted signal; A_s and A_w are the amplitudes of the frequency magnitude spectrum of the received signal in the presence of the sample and in water, respectively, and T is the transmission coefficient of the waves propagating through the front and rear surfaces of the sample, calculated as (Mischi et al., 2014):

$$T = \frac{2Z}{Z_w + Z} \cdot \frac{2Z_w}{Z_w + Z} = \frac{4Z_w Z}{(Z_w + Z)^2}, \tag{4}$$

where Z_w is the acoustic impedance of water.

The nonlinearity parameter B/A quantifies the distortion process of a finite-amplitude wave travelling through a medium (Cobb, 1983). The parameter B/A is obtained by approximating the pressure-density relation by the Taylor series up to the second order, and taking the ratio of the Taylor expansion coefficient of the quadratic term to that of the linear term (Gong et al., 1989). For the estimation of B/A of the phantom materials, high-pressure ultrasound pulses were transmitted using a transducer with 2.25-MHz center frequency (V306 with a diameter of 13 mm; Panametrics, Olympus Inc., Waltham, MA, USA) and received by a transducer with 5-MHz center frequency (V307 with a diameter of 25 mm; Panametrics, Olympus Inc., Waltham, MA, USA).

A comparative method using water as a reference was employed to estimate the nonlinearity parameter (Dong et al., 1999; Gong et al., 1989; Dunn et al., 1981; Zeqiri et al., 2015). The mathematical expressions for determining the B/A have been described in (Dong et al., 1999; Gong et al., 1989; Dunn et al., 1981; Zeqiri et al., 2015) based on a through-transmission experiment. In this type of experiment, the assumptions that ultrasonic sources can be modeled as plane waves, and the waves propagate in a lossless medium have often been employed. However, as mentioned in (Cobb, 1983), ultrasonic sources are not accurately modeled as plane waves sources due to diffraction, which may lead to inaccurate B/A estimates. To minimize the influence of diffraction on the measurements, we used a receiver

with larger surface area than the transmitter, adopting the concept from (Zeqiri et al., 2015).

Here, we aim at a relative comparison of B/A between different materials based on the same assumptions and the same experimental set-up; thus, we employed the plane-wave theory to model the ultrasound wave propagation by considering the fundamental and the second harmonic components only. Moreover, the model used here includes the nonlinear distortion occurring in the water path. As depicted in Figure 1, the wave propagation as well as the generation of the second harmonic component were divided into three parts. Part one is the path from the transmitter surface to the front surface of the sample, which consists of the attenuation of the initially transmitted signal and the generation of a second harmonic component because of the nonlinearity of water. Part two is the path within the sample. The fundamental and the generated second harmonic component from part one are attenuated. In addition, a new second harmonic component is generated due to the nonlinearity of the sample material. Part three is the path between the rear surface of the sample and the receiver, where the fundamental and the second harmonic components from the previous two parts are attenuated, and another second harmonic component is formed because of water.

Altogether, the received second harmonic component can be described as:

$$P_{2s1} = P_1^2(0)2\pi f q_w G_w(L_1) T_1 e^{-\alpha_{s2} d} T_2 e^{-\alpha_{w2} L_2}/2, \quad (5)$$

$$P_{2s2} = \left(P_1(0) e^{-\alpha_{w1} L_1} T_1\right)^2 2\pi f q_s G_s(d) T_2 e^{-\alpha_{w2} L_2}/2, \quad (6)$$

$$P_{2s3} = \left(P_1(0) e^{-\alpha_{w1} L_1} T_1 e^{-\alpha_{s1} d} T_2\right)^2 2\pi f q_w G_w(L_2)/2, \quad (7)$$

$$P_{2s} = P_{2s1} + P_{2s2} + P_{2s3}, \quad (8)$$

where

$$q = (\mathrm{B/A} + 2)/2\rho c^3 \quad (9)$$

and

$$G(x) = \left(e^{-2\alpha_1 x} - e^{-\alpha_2 x}\right)/(\alpha_2 - 2\alpha_1). \quad (10)$$

In the equations above, subscripts w and s refer to water and the sample, respectively; ρ is the density and c is the speed of sound in the medium; P_1 (0) is the peak acoustic pressure amplitude of the initially transmitted signal; L_1 and L_2 are the path length of part one and part three; f is the frequency of the transmitted signal; α_1 and α_2 indicate the attenuation coefficient at the fundamental and the second harmonic frequency in the unit of Np/m; and T_1 and T_2 refer to the transmission coefficients for the water-to-sample and sample-to-water interfaces, respectively, i.e.,

$$T_1 = \frac{2(\rho c)_s}{(\rho c)_w + (\rho c)_s} \quad (11)$$

and

$$T_2 = \frac{2(\rho c)_w}{(\rho c)_w + (\rho c)_s}. \quad (12)$$

As a reference, the received second harmonic component with only water is:

$$P_{2w} = P_1^2(0)2\pi f q_w G_w(L)/2, \quad (13)$$

where L is the distance between the transmitter and receiver.

The amplitude of the second harmonic for these two cases was obtained by performing the fast Fourier transform on the received signals with and without sample, respectively. The ratio of the second harmonic signals could then be derived as:

$$\mathrm{ratio}_{2f} = \frac{P_{2s}}{P_{2w}}. \quad (14)$$

Therefore

$$\frac{q_s}{q_w} = \frac{\mathrm{ratio}_{2f} \cdot G_w(L)}{\left(e^{-\alpha_{w1} L_1} T_1\right)^2 G_s(d) T_2 e^{-\alpha_{w2} L_2}} - \frac{G_w(L_1) T_1 e^{-\alpha_{s2} d} T_2 e^{-\alpha_{w2} L_2}}{\left(e^{-\alpha_{w1} L_1} T_1\right)^2 G_s(d) T_2 e^{-\alpha_{w2} L_2}} - \frac{\left(e^{-\alpha_{w1} L_1} T_1 e^{-\alpha_{s1} d} T_2\right)^2 G_w(L_2)}{\left(e^{-\alpha_{w1} L_1} T_1\right)^2 G_s(d) T_2 e^{-\alpha_{w2} L_2}}. \quad (15)$$

From Equation (15), the nonlinearity parameter B/A of the material sample in the term q_s can then be determined by using the nonlinearity parameter of water (B/A = 5.2 at room temperature) in combination with Equation (9) to obtain q_w.

Based on Equation (15), we proposed a ratio-distance model by repeating the B/A measurement with multiple L_2 ranging from 2 cm to 7 cm with a step of 1 cm, obtaining the corresponding ratio_{2f} at each L_2. In principle, for each sample, a same B/A value should be obtained at varying L_2 because the B/A of the material sample is invariant to L_2. Hence, with this model we performed a least square curve fitting to estimate the B/A value for each material sample.

For the phantom materials, two samples for each concentration of each material were tested. For the case materials, the nonlinearity measurement was not included because the case samples were thin and distortion effects can be neglected. For each material, the measurements were repeated three times at different times. The transmitted pulses were repeated multiple times for each condition, with a 0.25 ms time interval in between; therefore, the estimations

were averaged over multiple pulses to improve their accuracy. To validate our measurements, the acoustic properties of corn oil, commonly used as acoustic reference material, were also measured. The measured attenuation had an error within 0.1 dB/cm compared to literature values (Chanamai and McClements, 1998; Gong et al., 1989), and the B/A values (10.8 ± 0.8) were also in agreement with the properties reported in previous studies (Gong et al., 1989), confirming the reliability of the adopted measurements.

Ultrasound perfusion imaging experiment

(Micro)vascular phantoms having two crossed channels with diameter of 300 μm, from now on referred to as "perfusable phantoms", were fabricated using the wire-casting technique; by this technique, two wires with diameter of 300 μm were drawn out from the phantom after its solidification. The phantoms were made of PDMS 10:1 and PAA 20%, respectively. A syringe pump was used to provide a continuous UCA (SonoVue, Bracco, Milan, Italy) flow at a rate of 2 mL/min through the channels. CEUS imaging was then performed using a Verasonics ultrasound system (Verasonics Vantage 128, Verasonics Inc., Kirkland, USA) with a L11-4v probe transmitting at 3.5 MHz in contrast specific mode, combining the pulse inversion and amplitude modulation techniques. The applied acoustic pressure was quantified in terms of mechanical index (MI), which was set to 0.14 in this experiment. Power Doppler ultrasound imaging was also performed on both phantoms by using a Verasonics ultrasound system (Verasonics Vantage 128, Verasonics Inc., Kirkland, USA) with a L11-4v probe transmitting at 9 MHz at a Doppler pulse repetition frequency of 300 Hz. The power Doppler ultrasound images were obtained by taking the power of the acquired in-phase and quadrature data.

In addition, CEUS imaging was performed on a perfusion system made of TPX which is the optimal case material. The perfusion system contained two chambers, each with dimensions of 25 × 15 × 5 mm. The hydrogel (micro)vascular phantoms will be placed inside the chambers. The perfusion system aims at providing a protective case for the hydrogel (micro)vascular phantoms. As we know, hydrogel phantoms have in general a low mechanical stiffness and can be easily damaged during measurements. Moreover, (micro)vascular hydrogel phantoms have an inlet and outlet for flow perfusion; however, fixing the tubing in hydrogel phantoms is always problematic since the hydrogel materials are soft. By using such a perfusion system, the rigid connections can be fixed on the perfusion case, so that the phantoms remain intact. The perfusion system also allows for long-term imaging and storage of the soft hydrogel phantoms inside the case, with minimal dehydration of the hydrogel. To demonstrate the ultrasound transparency and usability of the perfusion system, a 500 μm channel phantom made of PAA 20% was placed inside the case. Then, a syringe pump was used to provide a continuous UCA (SonoVue, Bracco, Milan, Italy) flow at a rate of 0.4 mL/min through the channel. CEUS imaging was then performed using the same probe and imaging sequence aforementioned with the MI set to 0.2.

Scoring system

In order to quantitatively determine the optimal phantom and case material, a scoring system is designed to rank these materials in terms of their speed of sound, acoustic impedance, attenuation, nonlinearity, transparency, lifetime, stiffness, as well as preparation protocol. For phantom materials, the scoring criteria of acoustic properties are determined by using the acoustic properties of human soft tissues such as liver and breast. For case materials, considering that they are rigid materials, the scoring criteria of speed of sound and acoustic impedance are adjusted by expanding the acceptable range, but the criteria of attenuation are strictly determined according to the attenuation of human soft tissue. The transparency, life time and stiffness are classified based on long-term observation. Regarding the preparation protocol, typical materials, less common materials and the materials requiring extra process such as improving transparency will gain different scores. The scoring system is shown in Table 2.

RESULTS

Speed of sound (SoS) and Acoustic impedance (Z)

Figure 2 shows the measured SoS for seven phantom materials (agarose, alginate, gelatin, PAA, PVA, PEGDA and PDMS). The measured SoS is in the range from 1454 to 1512 m/s for agrarose, from 1420 to 1447 m/s for alginate, from 1495 to 1531 m/s for gelatin, from 1445 to 1538 m/s for PAA, from 1550 to 1616 m/s for PVA, from 1529 to 1576 m/s for PEGDA and from 1057 to 1081 m/s for PDMS. Moreover, the measured SoS in those materials indicates a trend with SoS increasing for higher concentration. The SoS values for agarose, PAA, PVA and PDMS with several known density are available in literature for comparison. For agarose with density of 1040 kg/m^3, an SoS of 1500 ± 30 m/s is reported (Zell et al., 2007). In our measurements, the SoS for agarose with density of 1032 kg/m^3 is 1499 ± 13 m/s. For PAA with density of 1024, 1052 and 1090 kg/m^3, SoS values of 1546 ± 2, 1595 ± 2, and 1580 ± 50 m/s, respectively, are reported (Prokop et al., 2003; Zell et al., 2007). In our measurements, the SoS for PAA with density of 1026 kg/m^3 is 1536 ± 2 m/s. For PVA with density of 1100 kg/m^3, the reported SoS is 1570 ± 20 m/s (Zell et al., 2007). In our case, the SoS for PVA with density of 1058 kg/m^3 is 1608 ± 9 m/s. Finally, for PDMS 10:1, an SoS between 1045 and 1060 m/s is reported by (Cafarelli et al., 2017); a value

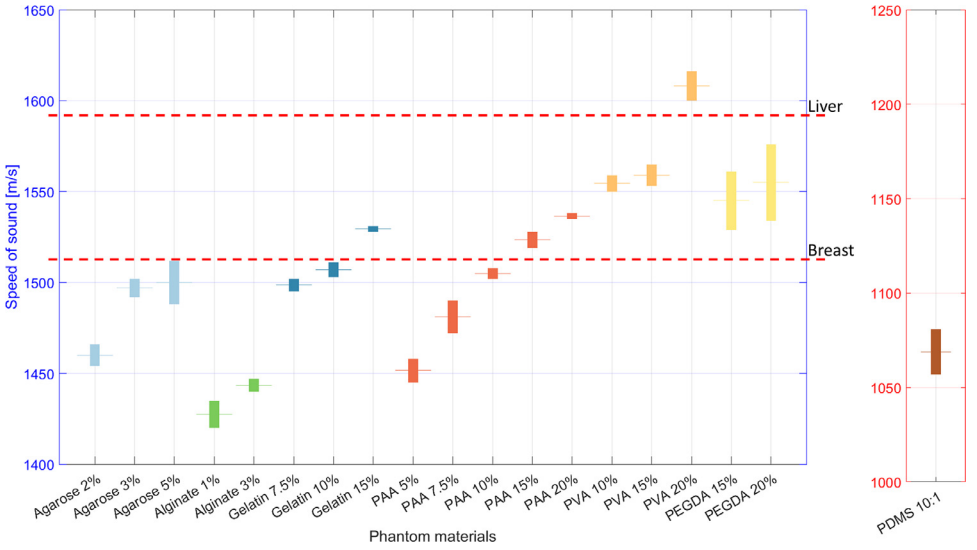

Figure 2. Measured speed of sound (SoS) of agarose, alginate, gelatin, PAA, PVA, PEGDA in varying concentrations, as well as of PDMS. The speed of sound (SoS) of liver and breast are also shown as reference. Note that the result of PDMS is separate because of the different scale. In each error bar, the mid-line and the bar indicate mean ± standard deviation.

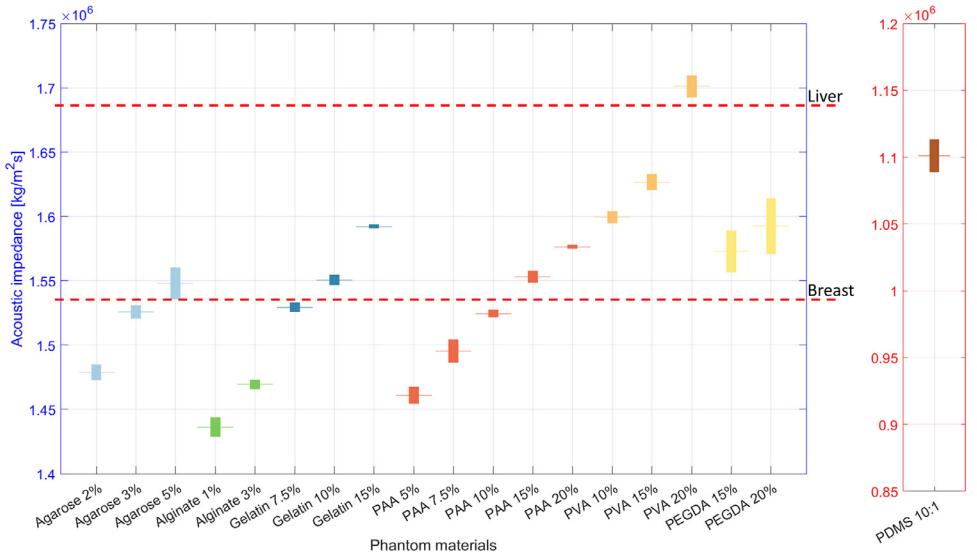

Figure 3. Measured acoustic impedance (Z) of agarose, alginate, gelatin, PAA, PVA, PEGDA in varying concentrations, as well as of PDMS. The acoustic impedance (Z) of liver and breast are shown as reference. Note that the result of PDMS is separate because of the different scale. In each bar, the mid-line and the length indicate mean ± standard deviation.

of 1030 m/s for PDMS is also mentioned by (Chen et al., 2016), but the density is unknown. In our test, the SoS for PDMS with density of 1030 kg/m^3 is 1068 ± 12 m/s.

Figure 3 shows the measured Z for the phantom materials. The measured Z ranges from 1.47 to 1.56 × 10^6 kg/m^{2}s for agarsose, from 1.43 to 1.47 × 10^6 kg/m^{2}s for alginate, from 1.53 to 1.59 × 10^6 kg/m^{2}s for gelatin, from 1.45 to 1.58 × 10^6 kg/m^{2}s for PAA, from 1.59 to 1.71 × 10^6 kg/m^{2}s for PVA, from 1.55 to 1.61 × 10^6 kg/m^{2}s for PEGDA, and from 1.09 to 1.11 × 10^6 kg/m^{2}s for PDMS. The measured Z increases for increasing material concentration. As reported in literature, for agarose with density of 1040 kg/m^3, the Z is 1.57 ± 0.08 × 10^6 kg/m^{2}s (Zell et al., 2007). In our measurements, the Z for agarose with density of 1032 kg/m^3 is 1.55 ± 0.014 × 10^6 kg/m^{2}s. For PAA with density of 1024, 1052 and 1090 kg/m^3, the Z values are 1.58 ± 0.008, 1.68 ± 0.004, and 1.73 ± 0.08 × 10^6 kg/m^{2}s, respectively (Prokop et al., 2003; Zell et al., 2007). In our case, the Z for PAA with density of 1026 kg/m^3 is 1.57 ± 0.002 × 10^6 kg/m^{2}s. For PVA with density of 1100 kg/m^3,

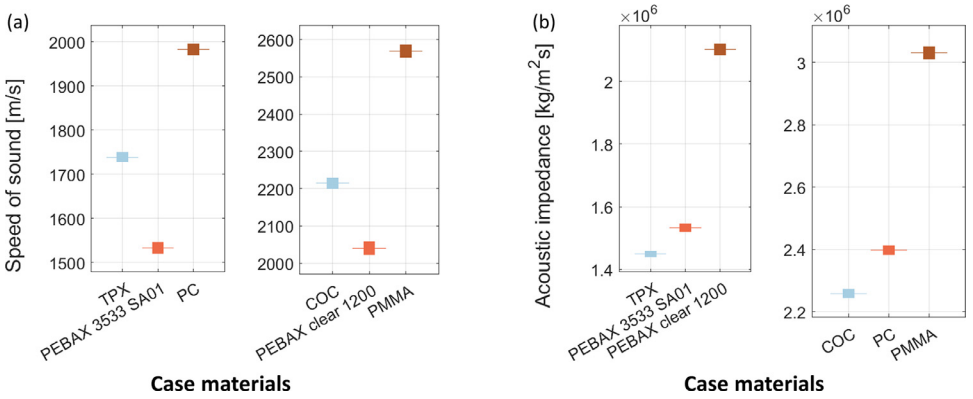

Figure 4. (a) and (b) are the measured speed of sound (SoS) and acoustic impedance (Z) of the case materials, respectively. Note that the results are shown separately because of the different scale. In each error bar, the mid-line and the bar indicate mean ± standard deviation.

the reported Z is 1.74 ± 0.08 × 10^6 kg/m^2s (Zell et al., 2007). In our work, the Z for PVA with density of 1058 kg/m^3 is 1.70 ± 0.009 × 10^6 kg/m^2s. For PDMS 10:1, a Z value between 1.08 and 1.10 × 10^6 kg/m^2s is reported by (Cafarelli et al., 2017). In our test, the Z for PDMS with density of 1030 kg/m^3 is 1.10 ± 0.01 × 10^6 kg/m^2s.

The measured SoS and Z for the case materials (PC, PMMA, TPX, COC and PEBA) are presented in Figure 4. The SoS of the case materials varies from 1520 to 2586 m/s, and the Z varies from 1.44 to 3.05 × 10^6 kg/m^2s.

Attenuation coefficient (α)

The measured α for the phantom materials at ultrasound frequencies varying from 1 MHz to 6 MHz are shown in Figure 5. The attenuation α for agarose, alginate, gelatin, PAA, PVA and PEGDA is within the range between about 0.10 and 2.26 dB/cm at frequencies varying from 1 MHz to 6 MHz. In contrast, PDMS shows a significantly higher α varying from about 2.96 to 22.18 dB/cm in the same frequency range. As expected, a clear trend can be observed with higher attenuation coefficient for higher frequency. In addition, α was compared between different concentrations for the same material at each frequency; for most cases, α increases with higher concentrations. As mentioned in (Zell et al., 2007), the acoustic attenuation coefficient for agarose with density of 1040 kg/m^3 is 0.4 ± 0.1 dB/cm at 5 MHz. In this work, the α for agarose with density of 1032 kg/m^3 was measured as 0.69 ± 0.13 dB/cm at 5 MHz. For PAA with density of 1024 and

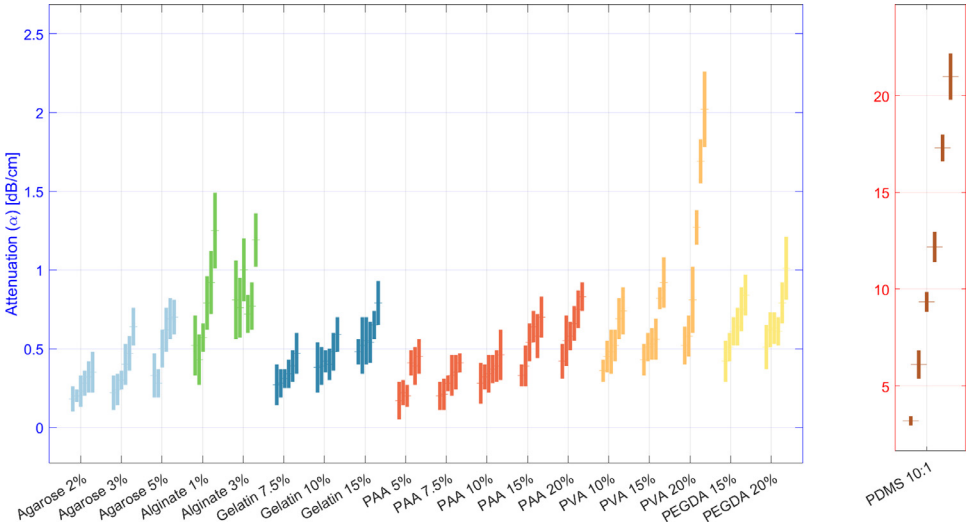

Figure 5. Measured attenuation coefficient (α) at frequencies ranging from 1 to 6 MHz of agarose, alginate, gelatin, PAA, PVA, PEGDA in varying concentrations. Note that the result of PDMS is separate because of the different scale. For each material, the set of measurement represents the α at varying frequencies. In each error bar, the mid-line and the bar indicate mean ± standard deviation.

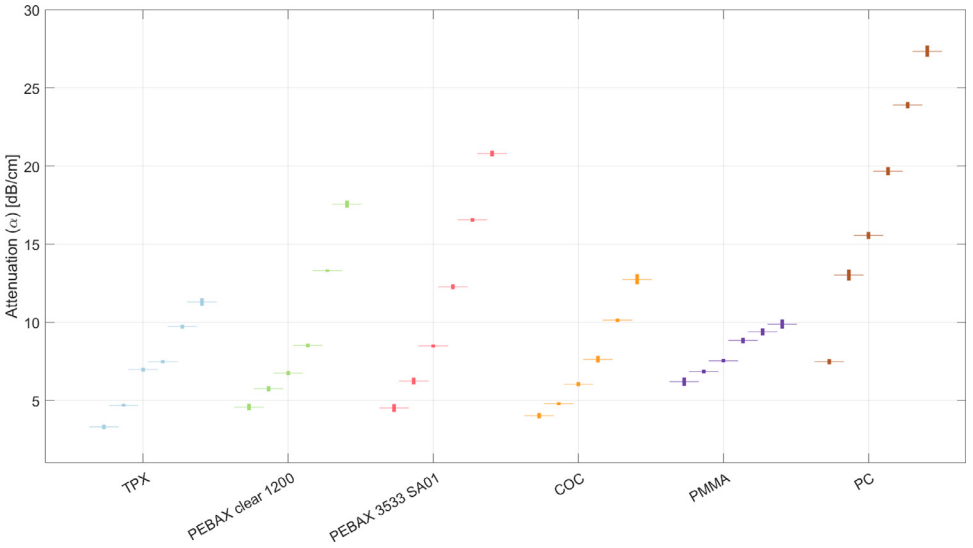

Figure 6. Measured attenuation coefficient (α) at frequencies ranging from 1 to 6 MHz of all the case materials. For each material, the set of measurement represents the α at varying frequencies. In each error bar, the mid-line and the bar indicate mean ± standard deviation.

1052 kg/m^3, the α varies from 0.08 ± 0.04 dB/cm to 0.44 ± 0.06 dB/cm and from 0.14 ± 0.02 dB/cm to 0.87 ± 0.04 dB/cm, respectively, at frequencies varying from 1 MHz to 5 MHz (Prokop et al., 2003). For PAA with density of 1090 kg/m^3, the measured α is 0.7 ± 0.1 dB/cm at 5 MHz (Zell et al., 2007). In our measurements, the attenuation coefficient for PAA with density of 1026 kg/m^3 varies from 0.42 ± 0.11 dB/cm to 0.75 ± 0.12 dB/cm at frequencies varying from 1 MHz to 5 MHz. In (Zell et al., 2007), the α for PVA with density of 1100 kg/m^3 is 2.9 ± 0.1 dB/cm at 5 MHz, while in our case the α is 1.69 ± 0.14 dB/cm at 5 MHz for PVA with density of 1058 kg/m^3. For PDMS 10:1, the α varies from 2.35 ± 0.28 to 16.58 ± 1.95 dB/cm at frequencies varying from 1 MHz to 5 MHz (Cafarelli et al., 2017), which is also comparable to our results.

The measured α of the case materials for frequencies varying from 1 MHz to 6 MHz is shown in Figure 6. The mean value of α varies from 3.30 dB/cm to 7.48 dB/cm at 1 MHz and varies from 9.88 dB/cm to 27.34 dB/cm at 6 MHz. According to expectations, the attenuation coefficient increases with increasing frequency. The value of α of the case materials is generally higher than that of the phantom materials. PC has higher α compared to other case materials. TPX and PMMA have relatively low α.

Figures 7 and 8 show the attenuation coefficient for all the phantom materials and case materials, respectively, measured at 3.5 MHz by using the two sets of transducers. The attenuation coefficient for liver and breast at 3.5 MHz are 1.75 dB/cm and 2.63 dB/cm, which are used as the reference. All the phantom materials have lower attenuation coefficient at 3.5 MHz compared to that of liver and breast, while all the case materials have higher attenuation coefficient at 3.5 MHz. The TPX has the lowest α at 3.5 MHz among the case materials.

Nonlinearity parameter (B/A)

Regarding the parameter of nonlinearity B/A, we first examined the nonlinear effect in the water path by conducting the experiments with varying distance between transmitter and receiver. As shown in Figure 9(a) and Figure 9(b), the amplitude of the fundamental frequency component does not show an obvious dependency on L; however, the amplitude of the second harmonic component increases with longer distance. Figures 9(c) and 9(d) illustrate the changes in the measured ratio$_{2f}$ with L_2 as well as a curve fitted to the proposed ratio-distance model (mentioned in the Materials and Methods Section) for PAA at a concentration of 20% and PDMS 10:1, respectively. The estimated B/A values for all phantom materials are reported in Figure 10. The B/A values for these phantom materials are rarely mentioned in literature. In (Zeqiri et al., 2015; Preobrazhensky et al., 2009), the B/A values of agar-based materials vary from 4.2 to 5.1, while (King et al., 2011; Casciaro et al., 2008) mentioned that the B/A values for hydrogels vary from 8.0 to 10.3. In this study, the phantom materials, except for PDMS, have B/A values approximately within the range from 5.0 to 12.0, which is the B/A values of soft tissues.

Ranking for materials

According to the criteria described in the scoring system (Table 2), all the phantom materials and case materials are ranked. The scores of all the materials are shown in

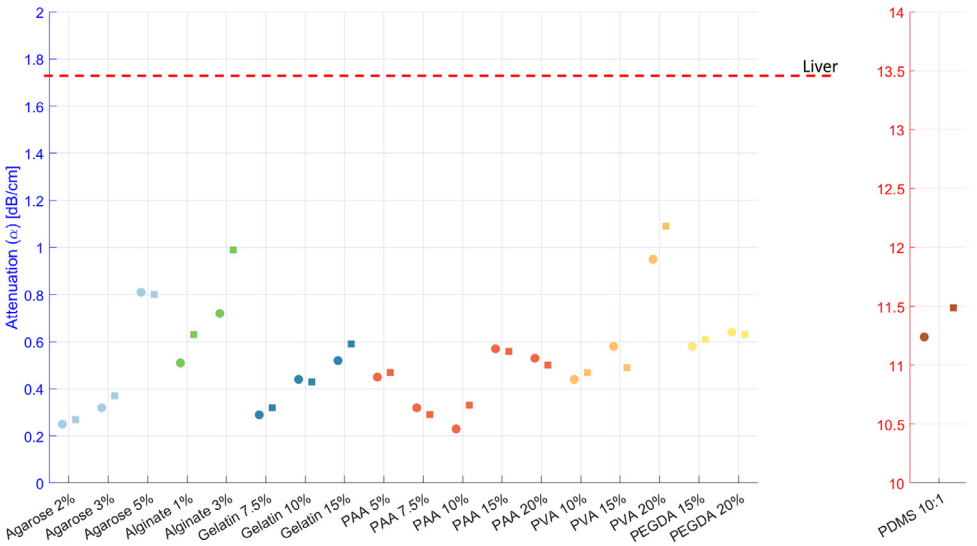

Figure 7. Measured attenuation coefficient (α) of all the phantom materials at 3.5 MHz by using the two sets of transducers. The attenuation coefficient (α) of liver are shown as reference. Note that the result of PDMS is separate because of the different scale. The circles indicate the measurement results by using the setup with low frequency range, while the squares indicate the results by using the setup with high frequency range.

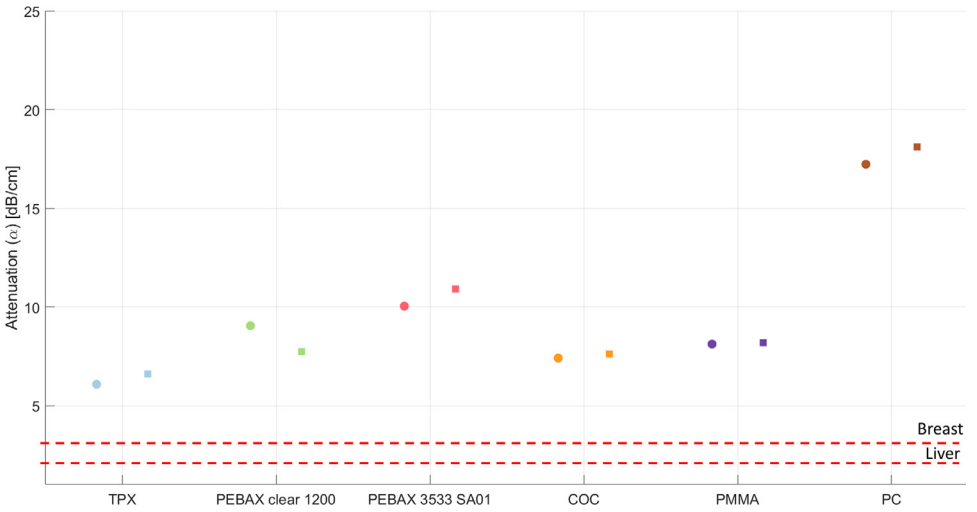

Figure 8. Measured attenuation coefficient (α) of all the case materials at 3.5 MHz by using the two sets of transducers. The attenuation coefficient (α) of liver and breast are shown as reference. The circles indicate the measurement results by using the setup with low frequency range, while the squares indicate the results by using the setup with high frequency range.

Table 3, in which the highest and lowest score are coded by yellow and red, respectively. The total score is 80. The PAA at a concentration of 20% gains 68.6, which is the highest score among phantom materials; therefore, the optimal phantom material is PAA 20%, while the PDMS 10:1 gains the lowest score of 37.0. For the case material, the optimal one is TPX with the score of 54.2.

Ultrasound perfusion imaging experiment

Examples of 300 μm crossed-channel phantoms made of PDMS 10:1 and PAA 20% are shown in Figures 11(a) and 11(d), respectively. The PDMS and PAA 20% obtain the lowest and highest score in the ranking aforementioned, respectively. Both PDMS and PAA have ideal optical transparency so that the channel structure can be clearly observed; however, CEUS imaging of the UCA flow in the channels is different for the two materials: Figure 11(b) shows one CEUS frame of the PDMS phantom, where the structure of the crossed channels is hard to observe because of the high attenuation of PDMS. In contrast, the UCA flow through the channels in the PAA phantom is clearly visible, as shown

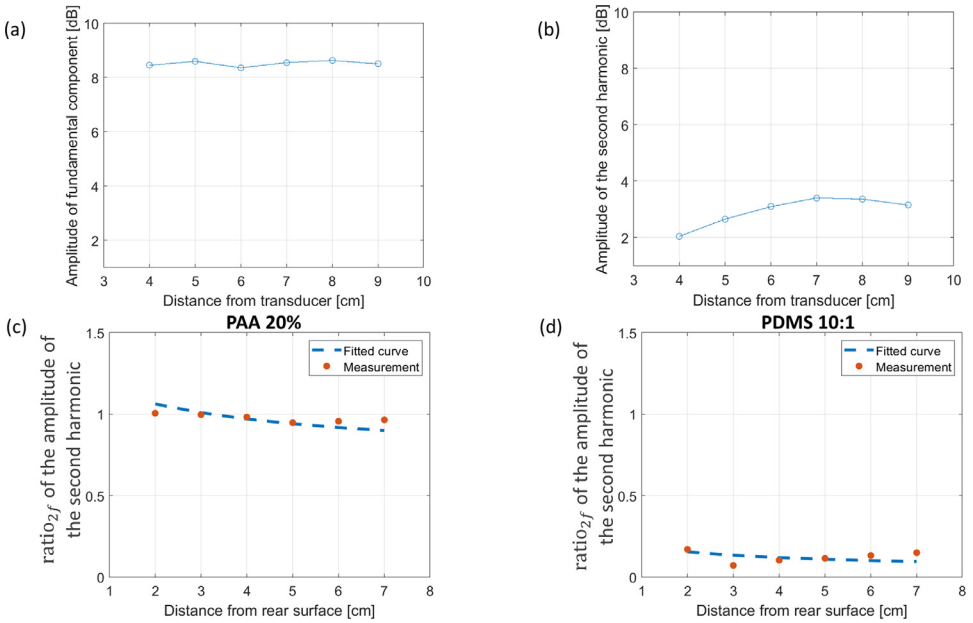

Figure 9. Nonlinearity parameter (B/A) estimation: (a) shows the amplitude of fundamental component in the frequency domain as a function of distance between transmitter and receiver; (b) shows the amplitude of the second harmonic component in the frequency domain as a function of distance between transmitter and receiver. (c) and (d) show the ratio$_{2f}$ of the second harmonic for the measured material sample and water as a function of L_2, including a fitted curve for PAA with a concentration of 20% and PDMS 10:1, respectively.

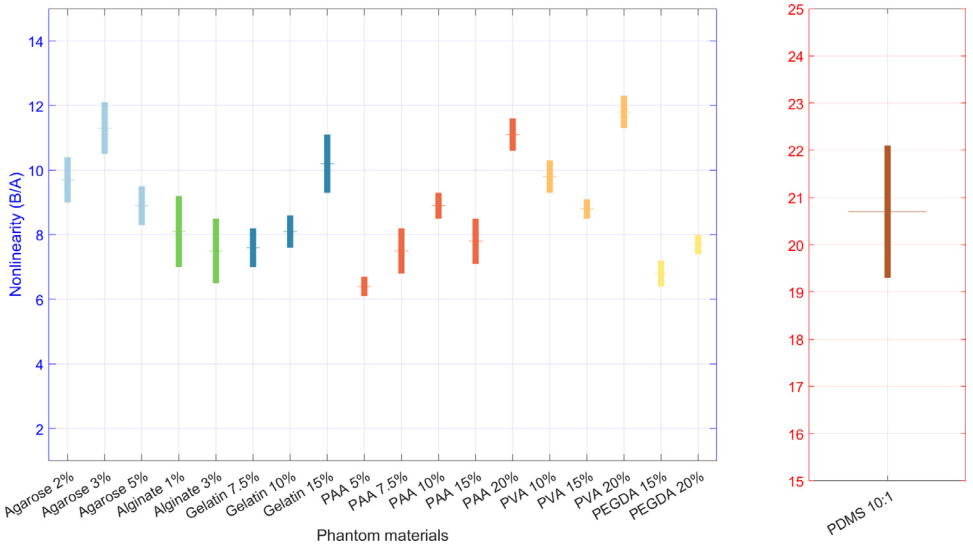

Figure 10. Measured acoustic nonlinearity (B/A) of agarose, alginate, gelatin, PAA, PVA, PEGDA in varying concentrations. Note that the result of PDMS is separate because of the different scale. In each error bar, the mid-line and the bar indicate mean ± standard deviation.

in Figure 11(e). In order to quantitatively compare figures 11(b) and 11(e), the contrast-to-background ratio was calculated by comparing the pixel intensity in two region-of-interests (yellow and red blocks) at the same imaging depth. For the PDMS phantom, the contrast-to-background ratio is 14.7 dB, while the ratio is 35.2 dB for the PAA 20% phantom.

In addition, one frame of the power Doppler ultrasound for the PDMS and PAA phantoms are shown in Figures 11 (c) and 11(f), respectively. The power Doppler ultrasound images also confirm that PAA has better acoustic properties than PDMS for the intended purpose.

Figures 12(a) and 12(b) depict an example of a perfusion system made of the optimal case material TPX,

Table 3. Ranking table for all the materials

Phantom material	Score
Agarose 2%	47.0
Agarose 3%	60.6
Agarose 5%	62.3
Alginate 1%	40.6
Alginate 3%	45.3
Gelatin 7.5%	56.2
Gelatin 10%	58.0
Gelatin 15%	63.5
PAA 5%	49.5
PAA 7.5%	55.8
PAA 10%	61.3
PAA 15%	63.4
PAA 20%	68.6
PVA 10%	60.5
PVA 15%	65.6
PVA 20%	63.9
PEGDA 15%	58.6
PEGDA 20%	63.7
PDMS 10:1	37.0
Case material	**Score**
TPX	54.2
PEBAX clear 1200	31.5
PEBAX 3533 SA01	50.0
COC	33.8
PMMA	33.1
PC	40.0

containing a single-channel PAA phantom inside one chamber. In Figure 12(c), CEUS imaging of the phantom chamber is presented. The UCA perfusion through the 500 μm channel can be well observed. Since the channel is horizontal, we cannot calculate the contrast-to-background ratio at the same imaging depth; therefore, two adjacent region-of-interests (yellow and red blocks) were placed inside the channel and outside the channel, representing the contrast and background respectively. The obtained ratio is 28.4 dB.

DISCUSSION

Preparation of materials

Gelatin and agarose are both widely used and easily available at low price. The process of making the phantoms is relatively easy, only involving dissolving the material and heating it before casting. Both materials come from a natural source and are not toxic but prone to molding and therefore not suitable for long term storage. The material properties are favourable for high percent agarose but the material remains brittle. Gelatin is hard to handle and will easily fall apart.

Alginate shows similarities with agarose and gelatin in properties but the cross-linking is achieved ionically and does not require any heating. This makes it a suitable alternative if higher temperatures are not possible during fabrication.

PAA is based on chemical cross-linking of the gel, making the process quick. Limitations with this process are in the toxic properties of the monomers and in that the reaction has to take place in a closed container to prevent inhibition via air. The resulting gel is transparent and mechanically stable at concentrations over 10% and it does not deteriorate over time. Overall, the material is ideal in all these properties but has to be handled carefully because of the potential presence of toxic monomers.

PDMS is one of the strongest materials we investigated, showing both optical transparency and long term storage even in dry conditions. The process of fabrication is simple but more time-consuming compared to the previous examples, and the cost is higher.

PVA is biocompatible and non-toxic. When an optically-transparent phantom is needed, gel fabrication is more time-consuming and more complex compared to other materials. By nature, PVA is a non-transparent hydrogel, which hampers optical imaging. Here, a transparent PVA hydrogel was obtained by performing low-temperature solidification overnight (Cha et al., 1992). Otherwise, the process is similar to that of gelatin and agarose and only involves dissolving and heating the material in water. The material properties are similar to PDMS but keeping the sample hydrated is essential for long-term storage.

PEGDA is similar to PAA in properties but uses photo-cross-linking and does not leave any toxic monomers. The process however is more elaborate than that for the other materials and requires a strong light source for crosslinking.

All case materials have good mechanical processing capabilities and can be made into the required shape. The costs for PMMA and PC are low and these materials are widely available. The other case materials that we investigated are more expensive and are not always available in the desired shape and size.

Acoustic properties, stability and longevity

The aim of this study was to determine the optimal tissue-mimicking phantom material compatible with

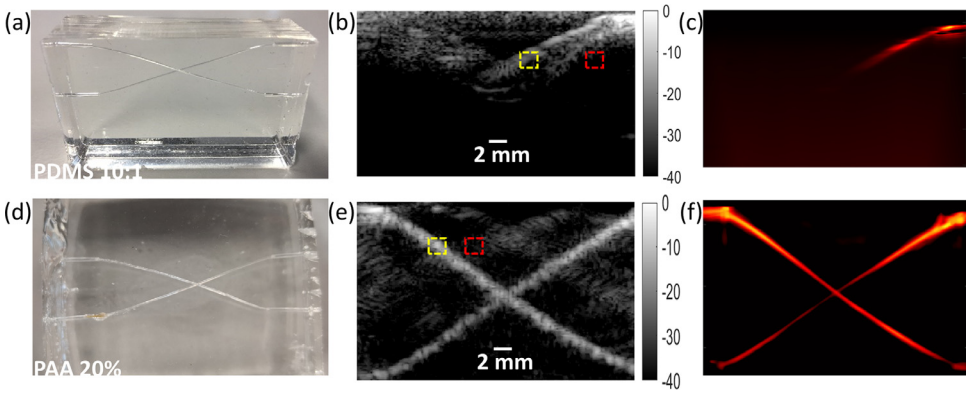

Figure 11. Perfusable phantom with two 300 μm non-connected crossed channels and the corresponding ultrasound perfusion images: (a) is the phantom made of PDMS 10:1; (b) is one CEUS frame of the PDMS phantom; (c) is one power Doppler ultrasound frame of the PDMS phantom; (d) is the phantom made of PAA with concentration of 20%; (e) is one CEUS frame of the PAA phantom; (f) is one power Doppler ultrasound frame of the PAA phantom. The region-of-interest of the contrast is indicated by the yellow block; while the region for background is indicated by the red block.

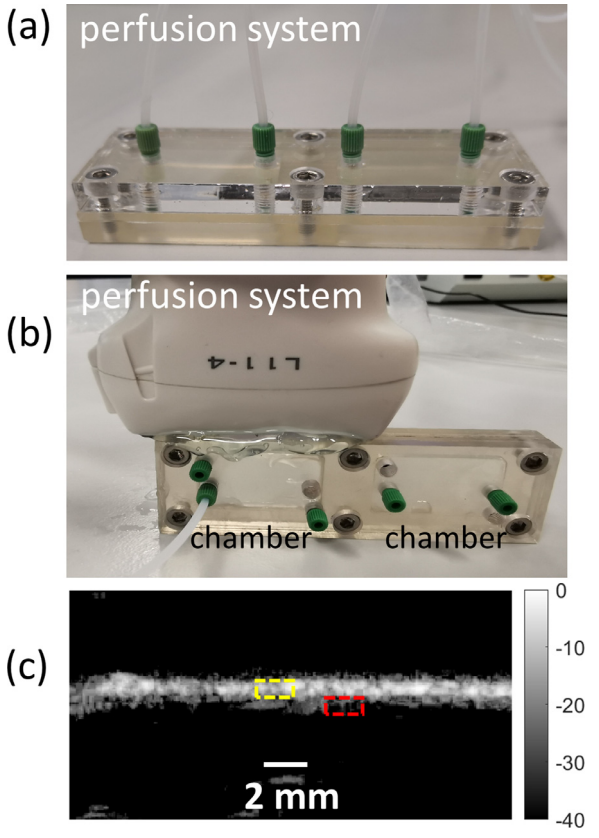

Figure 12. CEUS imaging of a perfusion system made of TPX: (a) and (b) show the perfusion system containing two chambers of dimensions 25 × 15 × 5 mm, and a single-channel PAA phantom is placed inside the chamber; (c) is the CEUS imaging of the chamber including the phantom. The visualization of UCA flow is presented. The region-of-interest of the contrast is indicated by the yellow block; while the region for background is indicated by the red block.

ultrasound perfusion imaging for perfusable phantoms, and optimal case materials for fixing the phantom. The phantom materials that were investigated for their acoustic properties are: agarose, alginate, gelatin, PAA, PVA, PEGDA and PDMS. Among them, a material with human-tissue-like acoustic properties as listed in Table 1, good longevity and stability, and a relatively easy preparation protocol would be our desired choice. A case material with the speed of sound and acoustic impedance close to that of the optimal phantom material and relatively low attenuation would be the optimal choice.

The speed of sound SoS values of phantom materials agarose, alginate, gelatin, PAA, PVA and PEGDA are around 1500 m/s, which is close to the SoS in soft human tissue (Culjat et al., 2010; Cao et al., 2017). Especially for gelatin with concentration of 15%, PAA with concentration of 15% and 20%, PVA with concentration of 10% and 15%, and PEGDA with concentration of 15% and 20%, the measured SoS is between 1510 and 1595 m/s; however, PDMS with a SoS of 1057 m/s was found to deviate largely from soft human tissue properties. For agarose, alginate, gelatin, PAA, PVA and PEGDA, the SoS increases with higher concentration because more concentrated materials are closer to a solid state rather than to a liquid state. The acoustic impedance Z of these materials, with the exception of PDMS, is similar to the impedance in human tissue as listed in Table 1. Especially for agarose with concentrations of 5%, gelatin with concentrations of 10% and 15%, PAA with concentration of 15% and 20%, PVA with concentration of 10% and 15%, and PEGDA with concentration of 15% and 20%, the acoustic impedance Z is between 1.54×10^6 and 1.69×10^6 kg/m^{2}s.

The measured SoS values of case materials TPX, PEBAX 3533 SA01 and PC are smaller than 2000 m/s, but

the SoS of PEBAX clear 1200, COC and PMMA deviate much from the SoS in soft human tissue. Considering the measured Z, only TPX and PEBAX 3533 SA01 have an acoustic impedance close to that of human soft tissue.

The attenuation coefficient α is a frequency-dependent parameter that increases with frequency, as measured for all these materials. Because of its high α, PDMS causes strong attenuation in depth and thus it is not a suitable phantom material. Since CEUS imaging is the most used modality to assess (micro)vascular perfusion, in this work, we particularly focused on materials that present higher contrast-to-background ratio for enhancing harmonic signal coming from UCA microbubbles; therefore, materials with attenuation higher than that of human tissue are not desirable. Based on the measurements, the α values of agarose, alginate, gelatin, PAA, PVA and PEGDA are smaller than 2.50 dB/cm in the frequency range varying from 1 MHz to 6 MHz, comparable to that of human tissue as listed in Table 1. The α of the case materials is relatively high since they are plastic materials with high mechanical stiffness. Among the tested case materials, TPX, COC and PMMA have lower α at frequencies of 4, 5 and 6 MHz. For all the materials, their α were measured at 3.5 MHz by using the two sets of transducers. For alginate, the difference between the two sets is 0.3 dB/cm. Since its attenuation coefficient is lower than 1 dB/cm, the difference is relatively large. Fabrication of thick and large alginate samples are problematic, which leads to the uncertainty of the measurement.

The parameter of nonlinearity B/A of gelatin, agarose, PAA, PVA, PDMS, alginate and PEGDA was determined by a curve-fitting method based on measurements at multiple sample-to-receiver (L_2) distances. Agarose, alginate, gelatin, PAA, PVA and PEGDA have B/A values ranging from 6.1 to 12.3, which are close to the B/A values of soft tissues, which range from 5.0 to 12.0. Other investigations have reported that agar-based tissue-mimicking materials had B/A values ranging from 4.2 to 5.1 (Zeqiri et al., 2015; Preobrazhensky et al., 2009); and hydrogel had B/A values ranging from 8.0 to 10.3 (King et al., 2011; Casciaro et al., 2008). Moreover, based on (Ma et al., 2004; Wu and Tong, 1998), the B/A value in UCA suspensions could reach several thousands, which is much higher than the B/A values mentioned above; thus, the B/A values of those tissue-mimicking materials will not have a strong influence in CEUS imaging. The results not only evidence that the materials can be used in CEUS imaging, since their coefficient of nonlinearity is lower than that of UCAs, but also give a comprehensive information about the B/A values of soft hydrogels, which also helps relevant research such as phantom-based ultrasound nonlinearity imaging. There is a special case for PDMS, with a measured B/A value over 20. However, the accuracy of this measurement may be influenced by the large difference between the SoS of PDMS and that of soft tissue, leading to high uncertainty in the B/A estimation using the proposed method. Moreover, as mentioned in (Cobb, 1983), media with high attenuation lead to significant errors in B/A measurement because the proposed method assumes that the acoustic wave propagates in a lossless medium. In general, the B/A estimation is sensitive to the values of measured α, SoS, and the transmitted and received signals. To reduce the uncertainty in the measurement, multiple measurements combining a least square curve fitting method were performed.

From the point of view of acoustic properties, for the phantom materials, PDMS is obviously not a suitable ultrasound-compatible material due to its low SoS and acoustic impedance, along with a high α. Morover, gelatin with concentrations of 15%, PAA with concentrations of 15% and 20%, PVA with concentrations of 10% and 15%, and PEGDA with concentration of 15% and 20% have acoustic properties closer to that of human soft tissue than the others. For the case materials, PEBAX clear 1200, COC and PMMA have high SoS, and are therefore unsuitable materials. Among TPX, PEBAX 3533 SA01 and PC, TPX has a relatively low α and the measured Z is close to that of human soft tissue.

Besides the acoustic properties, we also conducted one-month observation of those phantom material samples that were stored in a refrigerator under a humid environment. Obviously, the gelatin had the worst performance due to its easy microbial invasion. Microbial invasion was not observed in agarose, PVA and PEGDA samples, but they evidenced substantial deformation after one month of storage. PAA kept stable for long-term storage under the aforementioned environment. PDMS had the best longevity even if it was maintained at room temperature.

In addition, low mechanical stiffness of materials leads to fragile phantoms that are difficult to handle and perform experiments with; therefore, case materials with high mechanical strength are necessary. Among the phantom materials, alginate is a typical material with low mechanical stiffness. PEGDA, gelatin, low concentration PVA and low concentration PAA show relatively low mechanical stiffness as well. Agarose, high concentration PVA and PAA have higher stiffness, but they are softer than PDMS.

A good optical transparency enables the direct observation of designed microvasculature structures inside phantoms and optical imaging of perfusion by optical imaging systems. Poor transparency appeared in agarose, alginate and gelatin, compared with the other materials. Note that PVA is non-transparent by nature, but it became more transparent by our protocol, in

which solidification was done by keeping the PVA samples overnight at -20 degrees Celsius. Therefore, the preparation protocol of the PVA is more complicated than that of PAA.

By integrating all the assessments mentioned above and combining the ranking table, PAA 20% is our preferred choice as phantom material. To support our choice, we performed CEUS imaging of crossed-channel phantoms for both PAA 20% and PDMS 10:1. Because of the high α of PDMS, the deeper regions within the phantom were not visible in the ultrasound imaging. Moreover, strong artifacts along the channels were observed, because the SoS in PDMS is different from that of flowing UCA microbubbles. Conversely, CEUS imaging of UCA flowing through the crossed channels in PAA phantoms was well observed with contrast-to-background ratio of 35.2 dB; hence, PAA provides a promising phantom material for analysis of UCA dynamics.

The ranking table clearly shows TPX is the optimal choice as case material. TPX has a speed of sound at around 1700 m/s and relatively low acoustic impedance. Especially, its low attenuation would be the preferred choice. The CEUS imaging of the perfusion system also evidenced that the TPX case is compatible for ultrasound perfusion imaging by providing contrast-to-background ratio of 28.4 dB. The price of TPX is definitely higher than the price of the other case materials, as provided in Appendix B.

Although the reported measurements and analysis provide valuable insights for the fabrication of perfusion system including perfusable phantoms and their cases for Doppler ultrasound and CEUS imaging, this study presents several limitations. Firstly, for the nonlinearity measurement, as mentioned in (Dong et al., 1999; Zeqiri et al., 2015), a highly attenuated medium needs to be located close to the front surface of sample to meet the assumption that only the fundamental frequency signal travels through the sample. In our case, we considered the second harmonic signal generated between the transmitter and the sample in our estimation without placing a medium to remove harmonic signals. The B/A values of agarose, gelatin, PVA, PEGDA and PAA are expected to be close to the B/A values of soft tissue. To validate our method, we measured the nonlinearity of corn oil. The obtained results (10.8 ± 0.8) matched the values in literature. Second, although CEUS imaging of UCA flow in the PAA phantom comparing to the PDMS phantom supports our choice, the measurement of acoustic properties for UCA suspensions in other materials is worth further investigation. Moreover, fabrication of thick and large alginate samples remains troublesome, making the measurement results for this material uncertain. In this work, we measured the acoustic properties of the phantom materials in the frequency range from 1 to 6 MHz; however, this range does not fully cover the frequency we used in the ultrasound perfusion imaging experiments. Although the power Doppler ultrasound imaging results can evidence that the PAA is still compatible for ultrasound perfusion imaging at 9 MHz, the acoustic properties in higher frequency range are worth being measured. The thickness of phantom materials were measured by using a vernier caliper. Since the phantom materials are soft hydrogels, compressions from the vernier caliper may lead to small deformations of the soft hydrogels, which generates uncertainty in the thickness measurement. Moreover, large variations in temperature will lead to changes in acoustic properties of phantom materials. In this work, we submerged all the transducers and material samples in degassed water at a room temperature, and conducted all the experiments in a climate controlled room; therefore we assumed that the temperature is kept constant during the measurements. Taking additional steps to monitor and control temperature may facilitate more accurate measurements. Although the PAA 20% is determined as the optimal phantom material according to its good tissue-like properties, its attenuation is always lower than the attenuation of human tissue at high frequency range; as a result, this material may not optimally represent human tissue. But for the imaging purpose, lower attenuation is beneficial. The attenuation of the TPX is still high compared to the attenuation of soft hydrogels or human soft tissues, although the CEUS imaging results of the perfusion system show good visualization of the UCA flow. In order to minimize the influence of the high attenuation of TPX, the perfusion system can be further improved by reducing the thickness of the chamber wall.

CONCLUSIONS

In this study, a detailed analysis of tissue-mimicking phantom materials compatible for ultrasound perfusion imaging was performed based on experimental characterization of acoustic properties, long-term observation, as well as carrying out CEUS and power Doppler ultrasound imaging. In addition, the optimal case material for supporting the phantom was determined. We conclude that PAA and TPX are the optimal choice for phantom and case materials, respectively. Based on this choice, a complete perfusion system can be designed that allows for the *in-vitro* investigation of the relationship between UCA dynamics and the microvascular structure.

Acknowledgements—This work is supported by the research programme LOCATE with project number 15282, which is financed by the Dutch Research Council (NWO-TTW).

Conflict of interest disclosure—The authors have no conflict of interest to declare.

APPENDIX A. DENSITY OF THE PHANTOM AND CASE MATERIALS

Material	Density ρ (kg/m^3)	Source
Agarose 2%	1012.80	(Laurent, 1967)
Agarose 3%	1019.20	(Laurent, 1967)
Agarose 5%	1032.00	(Laurent, 1967)
Alginate 1%	1006.01	(Kamaruddin et al., 2014)
Alginate 3%	1018.03	(Kamaruddin et al., 2014)
Gelatin 7.5%	1020.63	(Winter and Shifler, 1975)
Gelatin 10%	1029.00	(Winter and Shifler, 1975)
Gelatin 15%	1041.00	(Winter and Shifler, 1975)
PAA 5%	1006.50	Supplier: Sigma-Aldrich
PAA 7.5%	1009.75	Supplier: Sigma-Aldrich
PAA 10%	1013.00	Supplier: Sigma-Aldrich
PAA 15%	1019.50	Supplier: Sigma-Aldrich
PAA 20%	1026.00	Supplier: Sigma-Aldrich
PVA 10%	1029.00	Supplier: Sigma-Aldrich
PVA 15%	1043.50	Supplier: Sigma-Aldrich
PVA 20%	1058.00	Supplier: Sigma-Aldrich
PEGDA 15%	1018.00	Supplier: Sigma-Aldrich
PEGDA 20%	1024.00	Supplier: Sigma-Aldrich
PDMS 10:1	1030.00	Supplier: Sylgard
TPX	834.00	Supplier: Sigma-Aldrich
PEBAX clear 1200	1030.00	Supplier: Arkema
PEBAX 3533 SA01	1000.00	Supplier: Arkema
COC	1020.00	Supplier: Topas
PMMA	1180.00	Supplier: Epraform
PC	1210.00	Supplier: Arla Plast AB

APPENDIX B. PRICE OF CASE MATERIAL

Case material	**Price per gram (Euro)**
TPX	0.218
PEBAX clear 1200	0.025
PEBAX 3533 SA01	0.063
COC	0.020
PMMA	0.001
PC	0.001

REFERENCES

Browne JE, Ramnarine KV, Watson AJ, Hoskins PR. Assessment of the acoustic properties of common tissue-mimicking test phantoms. Ultrasound Med. Biol. 2003;29:1053–1060.

Bude RO, Adler RS. An easily made, lowcost, tissuelike ultrasound phantom material. J. Clin. Ultrasound 1995;23:271–273.

Cafarelli A, Verbeni A, Poliziani A, Dario P, Menciassi A, Ricotti L. Tuning acoustic and mechanical properties of materials for ultrasound phantoms and smart substrates for cell cultures. Acta Biomaterialia 2017;49:368–378.

Caliari S, Burdick J. A practical guide to hydrogels for cell culture. Nature Methods 2016;13:405–414.

Cannon L, Fagan A, Browne JE. Novel tissue mimicking materials for high frequency breast ultrasound phantoms. Ultrasound Med. Biol. 2011;37:122–135.

Cao Y, Li GY, Zhang X, Liu YL. Tissue-mimicking materials for elastography phantoms: A review. Extreme Mechanics Letters 2017;17:62–70.

Casciaro S, Demitri C, Conversano F, Casciaro E, Distante A. Experimental investigation and theoretical modelling of the nonlinear acoustical behaviour of a liver tissue and comparison with a tissue mimicking hydrogel. J. Mater. Sci. Mater. Med. 2008;19:899–906.

Cha W, Hyon S, Ikada Y. Transparent poly(vinyl alcohol) hydrogel with high water content and high strength. Die Makromolekulare Chemie 1992;193:1913–1925.

Chanamai R, McClements D. Ultrasonic attenuation of edible oils. JAOCS, Journal of the American Oil Chemists' Society, 1998;75:1447–1448.

Chen A, Balter M, Chen M, Gross D, Alam S, Maguire T, Yarmush M. Multilayered tissue mimicking skin and vessel phantoms with tunable mechanical, optical, and acoustic properties. Medical Physics 2016;43:3117–3131.

Cobb WN. Finite amplitude method for the determination of the acoustic nonlinearity parameter b/a. J. Acoust. Soc. Am. 1983;73:1525–1531.

Cosgrove D. Ultrasound contrast agents: An overview. European Journal of Radiology 2006;60:324–330.

Cosgrove D, Lassau N. Imaging of perfusion using ultrasound. European Journal of Nuclear Medicine and Molecular Imaging 2010;37:65–85.

Culjat MO, Goldenberg D, Tewari P, Singh RS. A review of tissue substitutes for ultrasound imaging. Ultrasound Med. Biol 2010;36:861–873.

Dabbagh A, Abdullah BJJ, Ramasindarum C, Kasim NHA. Tissue-mimicking gel phantoms for thermal therapy studies. Ultrason. Imaging 2014;36:291–316.

Dong F, Madsen EL, MacDonald MC, Zagzebski JA. Nonlinearity parameter for tissue-mimicking materials. Ultrasound Med. Biol. 1999;25:831–838.

Dunn F, Law WK, Frizzell LA. Nonlinear ultrasonic wave propagation in biological materials. IEEE Ultrasonics symposium 1981;1981:527–532.

Dymling S, Persson H, Hertz C. Measurement of blood perfusion in tissue using doppler ultrasound. Ultrasound in Medicine and Biology 1991;17:433–444.

Feinstein S. The powerful microbubble: From bench to bedside, from intravascular indicator to therapeutic delivery system, and beyond. Am. J. Physiol. Heart Circ. Physiol. 2004;287:450–457.

Fromageau J, Brusseau E, Vray D, Gimenez G. Delachartre P. Characterization of pva cryogel for intravascular ultrasound elasticity imaging. IEEE Trans. Ultrason. Ferroelectr. Freq. Control 2003;50:1318–1324.

Funamoto K, Yamashita O, Hayase T. Poly(vinyl alcohol) gel ultrasound phantom with durability and visibility of internal flow. Journal of Medical Ultrasonics 2014;42:17–23.

Genchi G, Ciofani G, Liakos I, Ricotti L, Ceseracciu L, Athanassiou A, Mazzolai B, Menciassi A, Mattoli V. Bio/non-bio interfaces: A straightforward method for obtaining long term pdms/muscle cell biohybrid constructs. Colloids and Surfaces B: Biointerfaces 2013;105:144–151.

Gong X, Zhu Z, Shi T, Huang J. Determination of the acoustic nonlinearity parameter in biological media using fais and itd methods. J. Acoust. Soc. Am. 1989;86:1–5.

Havlice J, Taenzer J. Medical ultrasonic imaging: An overview of principles and instrumentation. Proceedings of the IEEE 1979;67:620–641.

Heintz K, Bregenzer M, Mantle J, Lee K, West J, Slater J. Fabrication of 3d biomimetic microfluidic networks in hydrogels. Advanced Healthcare Materials 2016;5:2153–2160.

Heintz K, Mayerich D, Slater J. Image-guided, laser-based fabrication of vascular-derived microfluidic networks. Journal of Visualized Experiments 2017;1–10.

ICRU. Tissue substitutes, phantoms, and computational modelling in medical ultrasound. : International Commission on Radiation Units Measurements; 1998.

Kamaruddin M, Yusoff M, Aziz H. Preparation and characterization of alginate beads by drop weight. International Journal of Technology 2014;5:121–132.

Kenwright DA, Laverick N, Anderson T, Moran CM, Hoskins PR. Wall-less flow phantom for high-frequency ultrasound applications. Ultrasound Med. Biol. 2015;41:890–897.

Kharine A, Manohar S, Seeton R, Kolkman R, Bolt R, Steenbergen W, de Mul F. Poly(vinyl alcohol) gels for use as tissue

phantoms in photoacoustic mammography. Phys. Med. Biol. 2003;48:357–370.
King RL, Liu Y, Maruvada S, Herman BA, Wear KA, Harris GR. Development and characterization of a tissue-mimicking material for high-intensity focused ultrasound. IEEE Trans. Ultrason. Ferroelectr. Freq. Control 2011;58:1397–1405.
Kuenen M, Mischi M, Wijkstra H. Contrast-ultrasound diffusion imaging for localization of prostate cancer. IEEE Trans. Med. Imaging 2011;30:1493–1502.
Laurent T. Determination of the structure of agarose gels by gel chromatography. Biochimica et Biophysica Acta - General Subjects 1967;136:199–205.
Law WK, Frizzell LA, Dunn F. Determination of the nonlinearity parameter b/a of biological media. Ultrasound Med. Biol. 1985;11:307–318.
Lee B, Ravindra P, Chan E. Size and shape of calcium alginate beads produced by extrusion dripping. Chemical Engineering and Technology 2013;36:1627–1642.
Ma J, Yu J, Fan Z, Zhu Z, Gong X, Du G. Acoustic nonlinearity of liquid containing encapsulated microbubbles. J. Acoust. Soc. Am. 2004;116:186–193.
Madsen E, Zagzebski J, Ghilardi-Netto T. An anthropomorphic torso section phantom for ultrasonic imaging. Medical Physics 1980;7:43–50.
Madsen EL, Frank GR, Dong F. Liquid or solid ultrasonically tissue-mimicking materials with very low scatter. Ultrasound Med. Biol. 1998;24:535–542.
Madsen EL, Zagzebski JA, Banjavie RA, Jutila RE. Tissue mimicking materials for ultrasound phantoms. Med. Phys. 1978;5:391–394.
Madsen EL, Zagzebski JA, Frank GR. Oil-in-gelatin dispersions for use as ultrasonically tissue-mimicking materials. Ultrasound Med. Biol. 1982;8:277–287.
Mast T. Empirical relationships between acoustic parameters in human soft tissues. Acoust. Res. Lett. Online-ARLO 2000;1:37–42.
Maxwell AD, Wang TY, Yuan L, Duryea AP, Xu Z, Cain CA. A tissue phantom for visualization and measurement of ultrasound-induced cavitation damage. Ultrasound Med. Biol. 2010;36:2132–2143.
Meagher S, Poepping TL, Ramnarine KV, Black RA, Hoskins PR. Anatomical flow phantoms of the nonplanar carotid bifurcation, part ii: Experimental validation with doppler ultrasound. Ultrasound Med. Biol. 2007;33:303–310.
Mischi M, Kuenen M, Wijkstra H. Angiogenesis imaging by spatio-temporal analysis of ultrasound contast agent dispersion kinetics. IEEE Trans. Ultrason. Ferroelectr. Freq. Control 2012;59:621–629.
Mischi M, Rognin N, Averkiou M. Ultrasound imaging modalities. Netherlands: Elsevier; 2014. p. 361–385.
Mischi M, Turco S, Soliman O, ten Cate F, Wijkstra H, Schoots I. Quantification of contrast kinetics in clinical imaging. : Springer; 2018.
Ophir J, Maklad NF, Jaeger PM. Patents assigned to acoustic standards corporation: Ultrasound phantom. patent number 1981; 4286455.
Preobrazhensky V, Pernod P, Pyl'Nov LK Y, Smagin N, Preobrazhensky S. Nonlinear acoustic imaging of isoechogenic objects and flows using ultrasound wave phase conjugation. Acta Acust. united with Acust. 2009;95:36–45.
Prokop AF, Vaezy S, Noble ML, Kaczkowski PJ, Martin RW, Crum LA. Polyacrylamide gel as an acoustic coupling medium for focused ultrasound therapy. Ultrasound Med. Biol. 2003;29:1351–1358.
Richardson C, Bernard S, Dinh VA. A cost-effective, gelatin-based phantom model for learning ultrasound-guided fine-needle aspiration procedures of the head and neck. J. Ultrasound Med. 2015;34:1479–1484.
Salsac A, Zhang L, Gherbezza J. Measurement of mechanical properties of alginate beads using ultrasound. 19th French Congress on Mechanics (CFM2009), 2009.
Shui G, Kim JY, Qu J, Wang YS, Jacobs LJ. A new technique for measuring the acoustic nonlinearity of materials using rayleigh waves. NDT E Int 2008;41:326–329.
Szabo T. Diagnostic Ultrasound Imaging: Inside Out. 2nd edition : Elsevier; 2014.
Turco S, Frinking P, Wildeboer R, Arditi M, Wijkstra H, Lindner J, Mischi M. Contrast-enhanced ultrasound quantification: From kinetic modeling to machine learning. Ultrasound in Medicine and Biology 2020;46:518–543.
van Sloun R, Demi L, Postema AW, Rosette JJDL, Wijkstra H, Mischi M. Entropy of ultrasound-contrast-agent velocity fields for angiogenesis imaging in prostate cancer. IEEE Trans. Med. Imaging 2017;36:826–837.
Wildeboer R, van Sloun R, Schalk S, Mannaerts C, van der Linden J, Huang P, Wijkstra H, Mischi M. Convective-dispersion modeling in 3d contrast-ultrasound imaging for the localization of prostate cancer. IEEE Trans. Med. Imaging 2018;37:2593–2602.
Winter J, Shifler D. The material properties of gelatin gels. : Ballistic Research Laboratories; 1975. p. 1–167 (BRL) Contractor Report No. 217 (AD-A008 396).
Wu J, Tong J. Measurements of the nonlinearity parameter b/a of contrast agents. Ultrasound Med. Biol. 1998;24:153–159.
Zell K, Sperl JI, Vogel MW, Niessner R, Haisch C. Acoustical properties of selected tissue phantom materials for ultrasound imaging. Phys. Med. Biol. 2007;52:475–484.
Zeqiri B, Cook A, Retat L, Civale J, Haar GT. On measurement of the acoustic nonlinearity parameter using the finite amplitude insertion substitution (fais) technique. Metrologia 2015;52:406–422.